







Trigonal distortion in zigzag-antiferromagnet iron phosphorus trisulfide

Aldrin G. Chang ^{1,2}, Liang-Wei Lan,¹ Yao-Jui Chan ^{1,3}, Chia-Nung Kuo,^{4,5} Ting Chen,¹ Chih-Heng Huang,¹ Tzu-Hung Chuang ⁶, Der-Hsin Wei ⁶, Chin-Shan Lue ^{4,5,7} and Chien-Cheng Kuo ^{1,*}

¹Department of Physics, National Sun Yat-sen University, Kaohsiung, Taiwan

²Physics Department, Technological University of the Philippines, Manila, Philippines

³Institute of Physics, Academia Sinica, Taipei, Taiwan

⁴Department of Physics, National Cheng Kung University, Tainan, Taiwan

⁵Taiwan Consortium of Emergent Crystalline Materials, National Science and Technology Council, Taipei, Taiwan

⁶National Synchrotron Radiation Research Center, Hsinchu, Taiwan

⁷Program on Key Materials, Academy of Innovative Semiconductor and Sustainable Manufacturing, National Cheng Kung University, Tainan, Taiwan



(Received 27 March 2022; revised 2 July 2022; accepted 8 August 2022; published 13 September 2022)

The electronic structure of FePS₃ was resolved using x-ray absorption spectroscopy with linear dichroism of x ray between in-plane and out-of-plane geometries. By integrating the measurements with semiempirical calculations, the observed nonvanishing feature in the dichroism spectra demands a site symmetry lower than cubic to be taken into account. These effects cause an energy splitting between a_{1g} and e_g^π orbitals of around 0.350 eV, contrary to previous reports purporting a smaller and insignificant energy splitting. Furthermore, reduction in the Slater integral was needed to establish agreement with experiment and theory suggesting metal-ligand covalency in the system. These findings shed light on how the local crystalline environment affects the electronic structure and the anisotropy in FePS₃ and will prove imperative in its potential spintronic applications.

DOI: [10.1103/PhysRevB.106.125412](https://doi.org/10.1103/PhysRevB.106.125412)

I. INTRODUCTION

Orbital occupation and the local environment play an essential role in determining the electronic and magnetic properties of materials [1,2]. How the electrons of an ion overlap and interact with the electrons of its neighboring ions is paramount in understanding the fundamental nature of materials [3–5], such as in metal-insulator transitions [6,7], magnetism [8,9], and superconductivity [10–12]. In MoS₂, the role of the local geometry in the spin and orbital structure was highlighted when a phase transition from the semiconducting trigonal prismatic phase to metallic octahedral phase yielded a decrease in the contact resistance in field-effect transistors [13]. In the negative charge transfer Mott insulator BaCoO₃ where the tetravalent Co ions are in the low-spin state, the hole in the e_g^π explained the observation of magnetocrystalline anisotropy [14].

The influence of these electronic properties is more pronounced in the two-dimensional (2D) magnetic materials which have received increased attention recently; specifically, the family of transition metal phosphorus trisulfides (MPS₃). The spin dimensionality in MPS₃ can be chosen by altering the metal, giving rise to systems explained by isotropic Heisenberg, anisotropic Heisenberg, and the 2D Ising model [15]. The [P₂S₆]⁴⁻ bipyramid is perpendicular

[Fig. 1(a)] to the metallic atoms arranged in a honeycomb lattice giving this family the moniker *magnetic graphene* [18]. MPS₃ was touted as a perfect two-dimensional magnetic material because of the negligible direct exchange and extremely weak magnetic interactions between layers [15]. A member of this family, iron phosphorus trisulfide (FePS₃), is a van der Waals material that crystallizes in the monoclinic symmetry, space group of $C_{2/m}$ [19]. It has an Ising-like spin dimensionality and a Néel temperature (T_N) of 118 K independent of thickness [15,20]. Fe²⁺ ions in this material are ferromagnetically coupled in a layer with two out of the three nearest neighbors and antiferromagnetically with the third one, forming zigzag magnetic ordering [21]. These zigzag chains couple antiferromagnetically [Fig. 1(b)] with the other chains within the layer and the ones along the c direction [22,23].

The optical absorption experiment claimed that the octahedra has a slight trigonal distortion, lowering the Fe-S local point group symmetry from O_h to D_{3d} . However, the trigonal field splitting (ΔD_{3d}) was purported to be negligible, just in the order of 10 meV [24]. This argument was negated by finding the material to be highly anisotropic using magnetic susceptibility [15] and three-dimensional torque magnetometry [25]. Neutron spectroscopy even estimated the trigonal splitting to be just 195 meV [26]. X-ray absorption spectroscopy (XAS) offers an advantage in resolving these controversial issues due to its capability in elucidating material character by showing strong resonance arising from the dipole-allowed transitions to unfilled valence states in an element-specific manner.

*Author to whom correspondence should be addressed: cckuo@mail.nsysu.edu.tw

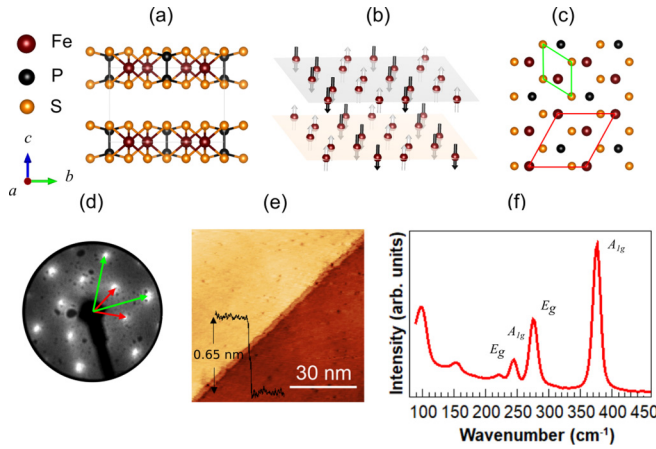


FIG. 1. (a) Atomic model of FePS₃ [16] rendered using VESTA [17] showing the atomic positions, (b) the spin configuration showing the zigzag-antiferromagnetic ordering, (c) periodicity of Fe and S unit cell viewed from the *c* axis, (d) LEED pattern obtained using beam energy of 48.5 eV showing the diffraction spots corresponding to the unit cell marked in (c), (e) STM image showing the step height, measured at 1.8 bias voltage and tunneling current of 900 pA, and (f) Raman spectrum using excitation wavelength of 532 nm and laser power of 5.8 mW.

In this work, we resolved the electronic structure due to the trigonal distortion and covalence between the Fe and S using polarization-dependent XAS and semiempirical calculations. This distortion causes energy splitting between a_{1g} and e_g^π orbitals of around 0.350 eV, evidenced by a non-negligible feature in the x-ray linear dichroism (XLD) between the in-plane and out-of-plane geometries. This feature manifested in both the magnetically ordered and disordered states, implying that the intensity distribution is predominantly induced by crystal-field effects and that no spin-state transition occurred. Considering Slater integral reduction, we further suggest a metal-ligand covalency in this material. These observations not only provide a clear insight into how the electronic structure is influenced by the local crystalline environment but is also essential in the material's potential spintronic application.

II. METHODOLOGY

Single crystals of FePS₃ were prepared using the chemical vapor transport method using sulfur as the transporting agent. High-purity phosphorus, sulfur, and iron powder were mixed thoroughly and were sealed in a quartz tube under high vacuum. The ampoule was heated for 1 to 2 wk in a horizontal two-zone furnace with a temperature gradient of 200 °C between 700 °C and 500 °C. In order to provide sufficient partial pressure for minimum transport rate and to ensure correct stoichiometry of obtained crystals, 3%–7% excess sulfur was necessary [27].

The unit cell periodicities of Fe and S are shown in Fig. 1(c) and manifested in the low energy electron diffractometry (LEED) [Fig. 1(d)]. The inner and outer diffraction spots have reciprocal lattice constants of 12.46 and 21.50 nm⁻¹, respectively. These correspond to the Fe and P unit cells shown in a red line, while the outer spots are for the S periodicity. Scan-

ning tunneling microscopy (STM) results [Fig. 1(e)] measured the terrace height to be about 0.65 nm. Raman spectroscopy was performed to verify the structure and vibrational properties of the sample. The Raman spectrum in Fig. 1(f) showed the E_g vibrational modes at 219.35 and 274.80 cm⁻¹ and the A_{1g} mode at 244.63 and 376.68 cm⁻¹. The peak located at around 99 cm⁻¹ corresponds to the Fe vibration band while the peak at around 153 cm⁻¹ is the infrared-active mode (E_u) of the P₂S₆ molecule [28,29].

III. RESULTS AND DISCUSSIONS

XAS was conducted using the total electron yield mode at the National Synchrotron Radiation Research Center, Taiwan Light Source 05B2 endstation with beamline geometry and optics discussed elsewhere [30]. The beam had a grazing incidence of 25° with respect to the sample surface as shown in Fig. 2(a). Room temperature (RT) in this experiment was about 300 K while low-temperature (LT) was about 110 K. The sample was exfoliated before loading to the ultrahigh vacuum chamber having a base pressure of 2×10^{-10} torr or better. Semiempirical calculations were performed to reveal the orbital ordering and hybridization [31].

Within an octahedral crystal field, the fivefold degenerate orbitals in spherical symmetry splits to an e_g doublet and t_{2g} triplet band with the latter being more stable [32]. The energy splitting between these two bands is known as the $10Dq$. Under a trigonal distortion, the cubic field elongates or contracts along the [111] direction [32,33] resulting in lifting of the degeneracy in the t_{2g} orbitals while the e_g orbitals remain doubly degenerate [32]. The t_{2g} band splits into a_{1g} and $e_{g\pm}^\pi$ orbitals where these states are linear combinations of d_{xy} , d_{yz} , and d_{xz} orbitals expressed as $|a_{1g}\rangle = \frac{1}{\sqrt{3}}(|xy\rangle + |yz\rangle + |xz\rangle)$ and $|e_{g\pm}^\pi\rangle = \pm \frac{1}{\sqrt{3}}(|xy\rangle + \exp(\mp \frac{2i\pi}{3})|yz\rangle + \exp(\pm \frac{2i\pi}{3})|xz\rangle)$. The wave function of a_{1g} has the same shape as the d_{z^2} orbital but is projected along the [111] direction while the $e_{g\pm}^\pi$ are perpendicular to this direction [33,34]. Possible ground-state orbital occupation is illustrated in Fig. 2(b). If $e_{g\pm}^\pi$ is more stable, a_{1g} has one hole.

The spectra of $2p$ XAS is a convolution of the intensity of the transition matrix elements given by

$$I \propto |\langle f|O|i\rangle|^2 \delta(E_f - E_i - \hbar\omega),$$

where the dipole operator O acts on the initial state $|i\rangle$ ($2p^6 3d^N$) and having a final state $|f\rangle$ ($2p^5 3d^{N+1}$). The delta function guarantees energy conservation such that the energy of the final state is the sum of the initial state and the incident photon energy. $2p$ XAS is dominated by electric dipole transitions in which the orbital quantum number of $|f\rangle$ differs by 1 from the $|i\rangle$ ($\Delta L = \pm 1$) and the spin is conserved ($\Delta S = 0$) [35–37]. The Fe L_3 (L_2) peak was found at 706.6 eV (719.3 eV) which is related to the electron excitation from the $2p_{3/2}$ ($2p_{1/2}$) level to an empty $3d$ state as shown in Fig. 2(c). Thus, the energy difference in $L_{3,2}$ peaks is related predominantly to the $2p$ spin-orbit coupling. The persistence of the dichroism in both paramagnetic and antiferromagnetic states as shown in Fig. 2(d) confirmed that the distribution has its origin dominated by crystal field. The overall negative intensity in the XLD spectra not only explains the transcen-

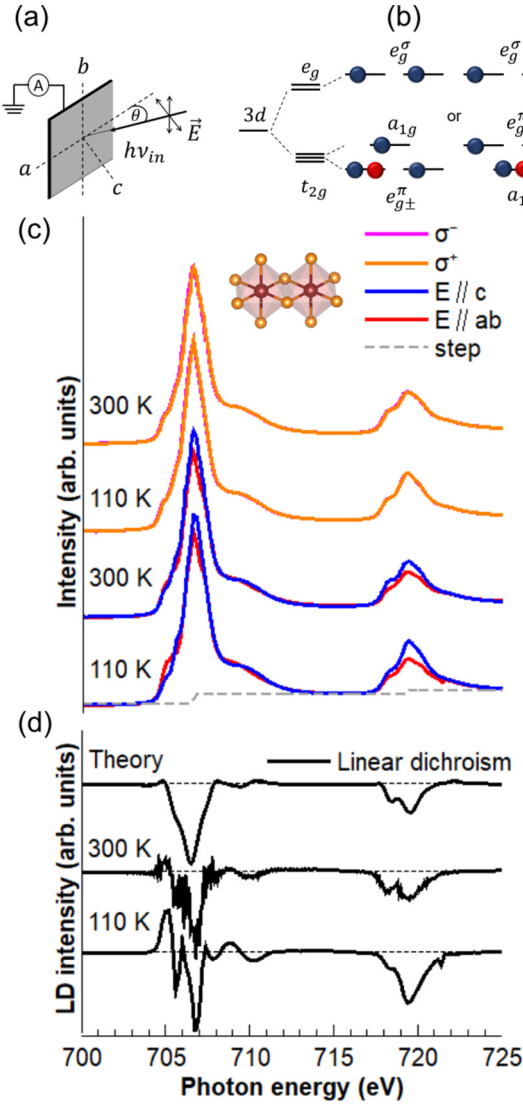


FIG. 2. (a) Cartoon for experimental geometry and the orientation of the sample with respect to the incoming light and (b) illustration of the electronic structure of the Fe^{2+} ion in FePS_3 showing the lifting of energy degeneracy due to trigonal distortion. Presented in (c) are the experimental spectra of Fe 2*p* XAS in FePS_3 using right (σ^-) circularly, left (σ^+) circularly, and linearly polarized light at 300 and 110 K. The inset illustrates the edge-sharing Fe-S octahedra. The gray dashed line is the two-step function used to remove the contribution from the continuum. (d) XLD ($\vec{E} \parallel ab$ - $\vec{E} \parallel c$) spectrum and its theoretical calculation simulated at 300 K. XAS using linearly polarized light has been corrected for geometry effects. Instrumental and core hole lifetime broadening were taken into account using a Gaussian of 0.10 eV and a Lorentzian of 0.36 (0.37) eV FWHM, respectively. Plots were arbitrarily shifted vertically for clarity.

dence from cubic symmetry but also explains the quadrupole moment and the local anisotropic charge distribution [38–40]. The positive feature at around 705 eV indicates that the lowest unoccupied orbital has an in-plane character and supports the situation that $e_{g\pm}^\pi$ is the lowest energy orbital.

Lifting the degeneracy in t_{2g} , the orbital ordering, and the energy separation that results in the trigonal distortion

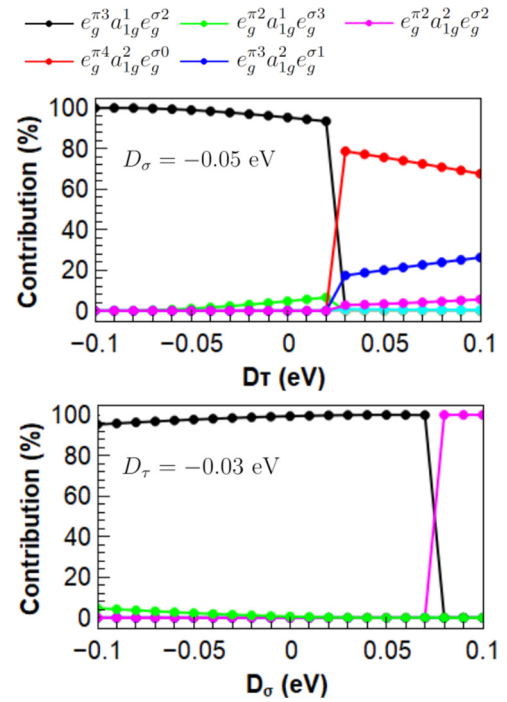


FIG. 3. Ground-state contribution as a function of trigonal distortion parameters.

were determined semiempirically. Ligand field multiplet theory (LFMT) developed by Thole *et al.* [41] was used. Built on the framework of the atomic multiplet theory established by Cowan and co-workers [42] and symmetry considerations by Butler [43], LFMT had successfully explained material properties strongly determined by symmetry in which perturbations due to the distribution of charges surrounding an isolated ion were explicitly taken into consideration. The matrix elements, upon the application of the trigonal to the cubic field, are given as

$$\langle e_g^\sigma | \mathcal{V} | e_g^\sigma \rangle = 6Dq + \frac{7}{3}D_\tau,$$

$$\langle e_{g\pm}^\pi | \mathcal{V} | e_{g\pm}^\pi \rangle = -4Dq + D_\sigma + \frac{2}{3}D_\tau, \quad \text{and}$$

$$\langle a_{1g} | \mathcal{V} | a_{1g} \rangle = -4Dq - 2D_\sigma - 6D_\tau,$$

where Dq , D_σ , and D_τ are the trigonal distortion parameters [32] and \mathcal{V} is the crystal-field potential energy considering the octahedral (\mathcal{V}_{oct}) and trigonal field (\mathcal{V}_τ): $\mathcal{V} = \mathcal{V}_{\text{oct}} + \mathcal{V}_\tau$. ΔD_{3d} is the energy splitting between a_{1g} and $e_{g\pm}^\pi$ quantified using the equation $\Delta D_{3d} = -3D_\sigma - 20D_\tau/3$. It is defined positive when the a_{1g} orbital is higher in energy or more unstable [44]. The trigonal distortion parameters were stepwise changed, having a good fit at $D_\sigma = -0.050$ eV and $D_\tau = -0.030$ eV corresponding to $\Delta D_{3d} = 0.350$ eV in comparison to optical spectroscopy value [45]. Representative calculations using a charge transfer multiplet program for XAS [46] are presented in Fig. 3. At $D_\sigma = -0.05$ eV, the ground-state contribution is dominated by $e_g^{\pi^3} a_{1g}^1 e_g^{\sigma^2}$ as D_τ was varied from -0.10 to 0.02 eV and at $D_\sigma \leq 0.07$ eV at $D_\tau = -0.03$ eV. Beyond these, the nature of the ground state will be that of a state with holes in the e_g^π as seen in the overall positive dichroism shown in Figs. S1(a), S1(e), and S1(f) of the

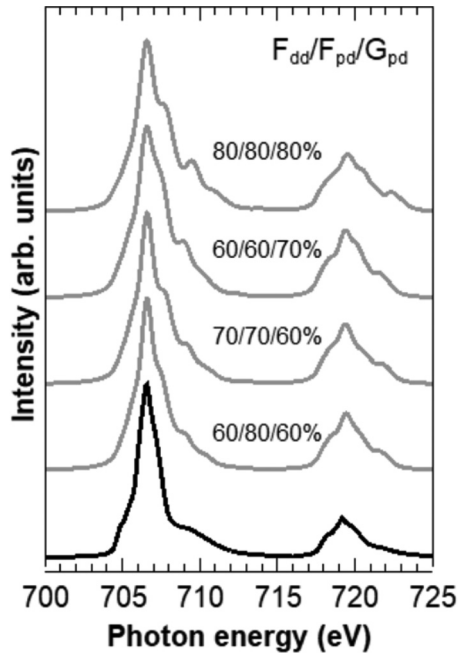


FIG. 4. Fitting of the isotropic experimental spectra (solid black line) with respect to the reduction of Slater integrals $F_{dd}/F_{pd}/G_{pd}$ implemented in the calculations (gray line). Agreement of theoretical calculations to experiment was established when the integral was reduced to 60/80/60%.

Supplemental Material [47]. The branching ratio represents the fraction of the L_3 transition to the total probability [48]. This is sensitive to the ground-state symmetry and spin state, making it also sensitive to the valence. The presence of a strong crystal field could result in a lower branching ratio when it produces an intermediate or low-spin ground state [49]. After normalization and edge jump subtraction, the branching ratio was found to be 0.79 in both the paramagnetic and antiferromagnetic ordering. This value is comparable to that of a high-spin Fe^{2+} [50]. The eigenvalue of the operator \hat{S}^2 is $6.0\hbar^2$ asserting the absence of any other spin states [51,52]. The XAS and XLD spectrum, the L_2 edge in particular, is better simulated if $3d$ spin-orbit coupling is not included [Fig. S2(a)] describing the quenched orbital angular momentum in this system with a 5E_g ground state. We attribute the difference in the XLD between RT and LT to the structural transition occurring at T_N characterized by a discontinuous change in lattice parameters [53].

Systematic peak width narrowing between pure transition metals and its oxides had been studied and conclusions drawn therein can be extended to the case of FePS_3 in light of hybridization [54,55]. We compared the half width at half maximum of metallic Fe and FePS_3 presented in Fig. S2(b) and we observed that FePS_3 L_3 is narrower by 30%. It is

customary to reduce the Slater integrals: the intra-atomic Slater (Coulomb) integrals of the Fe $3d$ electrons, F_{dd} ; the intra-atomic Slater (Coulomb) integrals of the Fe $2p$ and Fe $3d$ electrons, F_{pd} ; and the intra-atomic Slater exchange integrals of Fe $2p$ and Fe $3d$ electrons, G_{pd} to 80% of the atomic Hartree-Fock (HF) value to account for the excessive electron-electron repulsion found in the calculations of the free-ion case. However, this reduction was not enough to have the theoretical model agree with the experimental results, and thus, have to be further reduced to reflect electron delocalization and covalence. Representative percentage reduction of the Slater integrals, coded as $F_{dd}/F_{pd}/G_{pd}$ from HF values, are presented in Fig. 4. The Coulomb integrals can also be expressed in terms of the well-known Racah parameters B and C , specifically: $B = (9F_{dd}^2 - 5F_{dd}^4)/441$ and $C = 5F_{dd}^4/63$ [56]. We varied the Slater integrals and observed that 80% reduction in the G_{pd} manifests the least agreement in all combinations and must be lowered down to 60% to better fit with the experimental spectrum. Best reduction occurred at 60/80/60% reduction. Comparing also F_{dd} across at constant F_{pd} and G_{pd} , there is enhanced shoulder and peak width broadening leading us to the conclusion that the mentioned reduction resembles the best estimate within the assumptions in this work. Decreasing the Slater Coulomb integral (Racah B) to 60% of the free-ion value is the evidence regarding the nephelauxetic effect in this material.

IV. SUMMARY

In conclusion, this work provided evidence on the trigonal distortion in FePS_3 . The energy splitting in the t_{2g} orbital is around 0.350 eV. Additionally, the hybridization as manifested in the Slater integral reduction showed that FePS_3 has a covalent character. Furthermore, this work supports the observed magnetic anisotropy probed using torque magnetometry is due to the non-negligible trigonal crystal field. This work underlines the strength of XAS alongside multiplet calculations to probe the local electronic structure and hybridization in materials. Taking advantage of the large van der Waals gap and the ease in mechanical exfoliation, intercalation and heterostructures made from this material would be a good avenue to further explore possibilities with this 2D magnet.

ACKNOWLEDGMENTS

We acknowledge the support of the Ministry of Science and Technology of Taiwan (Grants No. 108-2112-M-110-010, No. 109-2112-M-110-020, and No. 110-2112-M-110-016). The authors would like to thank F. M. F. de Groot for the useful advice for the multiplet calculations and the research assistants in NSRRC BL05B2 EPU PEEM station for the help they extended during beamtimes.

[1] G. Fabbris, D. Meyers, J. Okamoto, J. Pellicciari, A. S. Disa, Y. Huang, Z.-Y. Chen, W. B. Wu, C. T. Chen, S. Ismail-Beigi, C. H. Ahn, F. J. Walker, D. J. Huang, T. Schmitt, and M. P. M. Dean, *Phys. Rev. Lett.* **117**, 147401 (2016).

[2] S. V. Streltsov and D. I. Khomskii, *Phys. Usp.* **60**, 1121 (2017).

[3] T. Saitoh, A. E. Bocquet, T. Mizokawa, and A. Fujimori, *Phys. Rev. B* **52**, 7934 (1995).

- [4] J. Zaanen, G. A. Sawatzky, and J. W. Allen, *Phys. Rev. Lett.* **55**, 418 (1985).
- [5] W. B. Wu, D. J. Huang, J. Okamoto, A. Tanaka, H.-J. Lin, F. C. Chou, A. Fujimori, and C. T. Chen, *Phys. Rev. Lett.* **94**, 146402 (2005).
- [6] M. W. Haverkort, Z. Hu, A. Tanaka, W. Reichelt, S. V. Streltsov, M. A. Korotin, V. I. Anisimov, H. H. Hsieh, H.-J. Lin, C. T. Chen, D. I. Khomskii, and L. H. Tjeng, *Phys. Rev. Lett.* **95**, 196404 (2005).
- [7] V. Bisogni, S. Catalano, R. J. Green, M. Gibert, R. Scherwitzl, Y. Huang, V. N. Strocov, P. Zubko, S. Balandeh, J.-M. Triscone, G. Sawatzky, and T. Schmitt, *Nat. Commun.* **7**, 13017 (2016).
- [8] J. Miyawaki, S. Suga, H. Fujiwara, M. Urasaki, H. Ikeno, H. Niwa, H. Kiuchi, and Y. Harada, *Phys. Rev. B* **96**, 214420 (2017).
- [9] A. Nag, H. C. Robarts, F. Wenzel, J. Li, H. Elnaggar, R.-P. Wang, A. C. Walters, M. García-Fernández, F. M. F. de Groot, M. W. Haverkort, and K.-J. Zhou, *Phys. Rev. Lett.* **124**, 067202 (2020).
- [10] M. Minola, G. Dellea, H. Gretarsson, Y. Y. Peng, Y. Lu, J. Porras, T. Loew, F. Yakhov, N. B. Brookes, Y. B. Huang, J. Pellicciari, T. Schmitt, G. Ghiringhelli, B. Keimer, L. Braicovich, and M. Le Tacon, *Phys. Rev. Lett.* **114**, 217003 (2015).
- [11] M. Hepting, D. Li, C. Jia, H. Lu, E. Paris, Y. Tseng, X. Feng, M. Osada, E. Been, Y. Hikita, Y. Chuang, Z. Hussain, K. Zhou, A. Nag, M. Garcia-Fernandez, M. Rossi, H. Huang, D. J. Huang, Z. Shen, T. Schmitt *et al.*, *Nat. Mater.* **19**, 381 (2020).
- [12] J. Zhang, A. Botana, J. Freeland, D. Phelan, H. Zheng, V. Pardo, M. Norman, and J. Mitchell, *Nat. Phys.* **13**, 864 (2017).
- [13] R. Kappera, D. Voiry, S. E. Yalcin, B. Branch, G. Gupta, A. D. Mohite, and M. Chhowalla, *Nat. Mater.* **13**, 1128 (2014).
- [14] Y. Y. Chin, Z. Hu, H.-J. Lin, S. Agrestini, J. Weinen, C. Martin, S. Hébert, A. Maignan, A. Tanaka, J. C. Cezar, N. B. Brookes, Y.-F. Liao, K.-D. Tsuei, C. T. Chen, D. I. Khomskii, and L. H. Tjeng, *Phys. Rev. B* **100**, 205139 (2019).
- [15] P. A. Joy and S. Vasudevan, *Phys. Rev. B* **46**, 5425 (1992).
- [16] A. Jain, S. P. Ong, G. Hautier, W. Chen, W. D. Richards, S. Dacek, S. Cholia, D. Gunter, D. Skinner, G. Ceder, and K. A. Persson, *APL Mater.* **1**, 011002 (2013).
- [17] K. Momma and F. Izumi, *J. Appl. Crystallogr.* **44**, 1272 (2011).
- [18] J.-G. Park, *J. Phys.: Condens. Matter* **28**, 301001 (2016).
- [19] G. Ouvrard, R. Brec, and J. Rouxel, *Mater. Res. Bull.* **20**, 1181 (1985).
- [20] J.-U. Lee, S. Lee, J. H. Ryoo, S. Kang, T. Y. Kim, P. Kim, C.-H. Park, J.-G. Park, and H. Cheong, *Nano Lett.* **16**, 7433 (2016).
- [21] A. R. Wildes, K. C. Rule, R. I. Bewley, M. Enderle, and T. J. Hicks, *J. Phys.: Condens. Matter* **24**, 416004 (2012).
- [22] M. Balkanski, M. Jouanne, G. Ouvrard, and M. Scagliotti, *J. Phys. C: Solid State Phys.* **20**, 4397 (1987).
- [23] B. L. Chittari, Y. Park, D. Lee, M. Han, A. H. MacDonald, E. Hwang, and J. Jung, *Phys. Rev. B* **94**, 184428 (2016).
- [24] P. A. Joy and S. Vasudevan, *Phys. Rev. B* **46**, 5134 (1992).
- [25] M. Nauman, D. H. Kiem, S. Lee, S. Son, J.-G. Park, W. Kang, M. J. Han, and Y. Jo, *2D Mater.* **8**, 035011 (2021).
- [26] K. C. Rule, A. R. Wildes, R. I. Bewley, D. Visser, and T. J. Hicks, *J. Phys.: Condens. Matter* **21**, 124214 (2009).
- [27] A. Dhanarajgopal, P.-C. Chang, S.-Y. Liu, T.-H. Chuang, D.-H. Wei, C.-C. Kuo, C.-N. Kuo, C. S. Lue, and W.-C. Lin, *Appl. Surf. Sci.* **567**, 150864 (2021).
- [28] C. C. Mayorga-Martinez, Z. Sofer, D. Sedmidubský, Å. Huber, A. Y. S. Eng, and M. Pumera, *ACS Appl. Mater. Interfaces* **9**, 12563 (2017).
- [29] G. Herzberg, Jr. and B. L. Crawford, *J. Phys. Chem.* **50**, 288 (1946).
- [30] D. Wei, Y.-L. Chan, and Y.-J. Hsu, *J. Electron Spectrosc. Relat. Phenom.* **185**, 429 (2012).
- [31] E. Stavitski and F. M. de Groot, *Micron* **41**, 687 (2010).
- [32] C. Ballhausen, *Introduction to Ligand Field Theory*, McGraw-Hill Series in Advanced Chemistry (McGraw-Hill, New York, 1962).
- [33] D. I. Khomskii, *Transition Metal Compounds* (Cambridge University Press, Cambridge, UK, 2014).
- [34] B. Pal, Y. Cao, X. Liu, F. Wen, M. Kareev, A. T. N'Diaye, P. Shafer, E. Arenholz, and J. Chakhalian, *Sci. Rep.* **9**, 1896 (2019).
- [35] F. de Groot, *Coord. Chem. Rev.* **249**, 31 (2005).
- [36] G. van der Laan and A. I. Figueroa, *Coord. Chem. Rev.* **277-278**, 95 (2014).
- [37] J. Stöhr and H. C. Siegmann, *Magnetism*, Springer Series in Solid-State Sciences (Springer-Verlag, Berlin/Heidelberg, 2006).
- [38] P. Schofield, G. D. Laan, C. Henderson, and G. Cressey, *Mineral. Mag.* **62**, 65 (1998).
- [39] J. Okabayashi, Y. Iida, Q. Xiang, H. Sukegawa, and S. Mitani, *Appl. Phys. Lett.* **115**, 252402 (2019).
- [40] P. Carra, H. König, B. Thole, and M. Altarelli, *Phys. B: Condens. Matter* **192**, 182 (1993).
- [41] B. T. Thole, G. van der Laan, J. C. Fuggle, G. A. Sawatzky, R. C. Karnatak, and J.-M. Esteve, *Phys. Rev. B* **32**, 5107 (1985).
- [42] R. Cowan and University of California Press, *The Theory of Atomic Structure and Spectra*, Los Alamos Series in Basic and Applied Sciences (University of California Press, Berkeley, 1981).
- [43] P. H. Butler, *Point Group Symmetry Application, Methods and Tables*, 1st ed. (Plenum Press, New York, 1981).
- [44] H.-J. Lin, Y. Y. Chin, Z. Hu, G. J. Shu, F. C. Chou, H. Ohta, K. Yoshimura, S. Hébert, A. Maignan, A. Tanaka, L. H. Tjeng, and C. T. Chen, *Phys. Rev. B* **81**, 115138 (2010).
- [45] N. Nagasundaram and A. Francis, *J. Phys. Chem. Solids* **50**, 163 (1989).
- [46] M. U. Delgado-Jaime, K. Zhang, J. Vura-Weis, and F. M. F. de Groot, *J. Synchrotron Radiat.* **23**, 1264 (2016).
- [47] See Supplemental Material at <http://link.aps.org/supplemental/10.1103/PhysRevB.106.125412> for the additional comparisons between the $2p$ XAS of Fe in FeP₃ and its theoretical simulation.
- [48] B. T. Thole and G. van der Laan, *Phys. Rev. B* **38**, 3158 (1988).
- [49] F. De Groot and A. Kotani, *Core Level Spectroscopy of Solids*, Advances in Condensed Matter Science (Taylor & Francis Group, Boca Raton, 2008).
- [50] G. van der Laan and B. T. Thole, *Phys. Rev. B* **43**, 13401 (1991).
- [51] M. Retegan, Crispy: v0.7.3, 2019.
- [52] M. W. Haverkort, M. Zwierzycki, and O. K. Andersen, *Phys. Rev. B* **85**, 165113 (2012).

- [53] P. Jernberg, S. Bjarman, and R. Wäppling, *J. Magn. Magn. Mater.* **46**, 178 (1984).
- [54] R. D. Leapman, L. A. Grunes, and P. L. Fejes, *Phys. Rev. B* **26**, 614 (1982).
- [55] J. Chen, *Surf. Sci. Rep.* **30**, 1 (1997).
- [56] M. O. Hunault, Y. Harada, J. Miyawaki, J. Wang, A. Meijerink, F. M. F. de Groot, and M. M. van Schooneveld, *J. Phys. Chem. A* **122**, 4399 (2018).